Applied Catalysis B: Environmental 142–143 (2013) 423–431

Contents lists available at SciVerse ScienceDirect

Applied Catalysis B: Environmental

journal homepage: www.elsevier.com/locate/apcatb

Rhodium supported on tetragonal or monoclinic ZrO_2 as catalyst for the partial oxidation of methane

M.C. Campa [a], G. Ferraris [a], D. Gazzoli [b], I. Pettiti [b,*], D. Pietrogiacomi [b]

[a] Istituto per lo Studio dei Materiali Nanostrutturati-CNR, c/o Dipartimento di Chimica, "Sapienza" Università di Roma, Piazzale Aldo Moro 5, 00185 Roma, Italy

[b] Dipartimento di Chimica, "Sapienza" Università di Roma, Piazzale Aldo Moro 5, 00185 Roma, Italy

ARTICLE INFO

Article history:
Received 8 March 2013
Received in revised form 17 May 2013
Accepted 22 May 2013
Available online 29 May 2013

Keywords:
Methane catalytic partial oxidation
Rh/ZrO_2 catalysts
FTIR characterization
Rh dispersion

ABSTRACT

The catalytic partial oxidation (CPO) of methane on Rh/ZrO_2 catalysts was investigated at different Rh loading (0.04–3.3 wt%), by using both monoclinic (m-ZrO_2) and tetragonal (t-ZrO_2) zirconia as supports. m-ZRhx and t-ZRhx catalysts, were prepared by dry impregnation of zirconia supports with a solution of $Rh(NO_3)_3$, and characterized by XRD, BET analysis, XPS, FTIR spectroscopy (using CO as probe molecule) and H_2/O_2 titration. CPO of methane was studied in a flow apparatus fed by a reactant mixture of $CH_4{:}O_2 = 2{:}1\%$ (v/v) in N_2 (contact time $\tau \simeq 2$ ms).

Characterization results show that the nature and dispersion of supported Rh species strongly depends on the support. The H_2/O_2 titration showed that Rh species are more dispersed on t-ZrO_2 than on m-ZrO_2. The XPS results indicated the presence of Rh in the metallic state both in large and small $Rh^{\delta+}$ clusters. Consistently with XPS, FTIR with CO probe molecule revealed the coexistence of Rh^0-CO carbonyls on Rh^0 large particles and Rh^+-$(CO)_2$ dicarbonyls arising from very small clusters. Rh species in the metallic state are more homogeneous (i.e. Rh^0 species with similar near-neighbor atoms) and Rh species with a lower metal character (i.e. those interacting with the support) are more abundant in the t-ZRhx samples than in the m-ZRhx ones.

For methane CPO, Rh supported on the tetragonal zirconia is far more active and selective than Rh supported on the monoclinic zirconia. The catalytic results suggest that the different Rh dispersion alone cannot account for the different catalytic performances of the t-ZRhx and m-ZRhx samples.

1. Introduction

Catalytic partial oxidation (CPO) of methane to syngas has attracted considerable interest as a way to use natural gas resources as well as biomass sources and possibly to contribute to a carbon-neutral energy chain [1–4]. Although the partial oxidation of methane has been known for a long time [1], the growing interest in this mildly exothermic reaction has resulted from the observation that high methane conversion and syngas selectivity with H_2/CO molar ratio around 2 can be achieved over noble metal-based catalysts running the process autothermally at short contact time [5,6]. Among the various metals (Rh, Pd, Pt, Ni and Ru) on different supports, investigated as catalysts for partial oxidation of methane to syngas [1,4–18], Rh is recognized to provide the best performances in terms of activity, syngas selectivity and resistance to coke deposition [5,19,20]. By consensus [2], on Rh-supported catalysts the presence of metallic Rh species is crucial for the methane CPO. Although many studies have been done regarding the influence of the catalyst features on the catalytic behavior [21–26] and to understand the reaction mechanisms [27–30], several aspects including the physicochemical properties of the active site, the role of the support in the metal-support interaction and in the reaction mechanism are still unclear.

For catalysts based on oxide-supported metal particles, one of the most important factors determining the performances of the catalytic systems is the interaction of the metal particles with the support [31–33]. It has been shown that the interaction strength at the metal-support interfaces can modify the shape and size of metal particles, resulting in species that exhibit different properties from those of bulk metals. Moreover, changes of the geometric and electronic properties with the particles size can induce the formation of specific active sites on the metal particle periphery composed of the metal site and the site on the support surface [34–38].

Zirconium oxide has received considerable attention as a catalyst support owing to its amphoteric surface properties and its stability under oxidizing and reducing environments [39]. The physico-chemical properties of zirconia, including structure, surface area, pore structure and acid–base characteristics, can be tailored according to preparation method and thermal treatments [40,41]. ZrO_2 exhibits three different polymorphs, monoclinic

* Corresponding author. Tel.: +39 06 49913378; fax: +39 06 490324.
E-mail address: ida.pettiti@uniroma1.it (I. Pettiti).

0926-3373/$ – see front matter © 2013 Elsevier B.V. All rights reserved.
http://dx.doi.org/10.1016/j.apcatb.2013.05.046

(m-ZrO_2), tetragonal (t-ZrO_2) and cubic (c-ZrO_2) and low temperature stabilized t-ZrO_2 and c-ZrO_2 forms. Among them, in the catalytic field attention is mainly given to m-ZrO_2, to low temperature stabilized t-ZrO_2 form and to a mix of monoclinic and tetragonal phases [42–45].

Although the effect of the monoclinic or tetragonal phase on the catalytic performance of zirconia-based catalysts has been found for a number of reactions [42–45], to the best of our knowledge the influence of crystal structures on CPO of methane has not been investigated. Bell et al. found that the Cu/m-ZrO_2 catalysts exhibit higher activity and selectivity than Cu/t-ZrO_2 systems for methanol synthesis [42,43]. Wang et al. [44] also reported that the surface-enriched monoclinic phase on the surface of tetragonal zirconia has beneficial effects for methanol steam reforming performed on Cu/ZrO_2 catalysts. The results obtained by Benito et al. [45] for ethanol steam reforming on Ni, Co and Cu supported on zirconia with monoclinic and tetragonal structure, indicate that nickel supported on tetragonal zirconia exhibited the best stability and selectivity to hydrogen production. The different behavior shown by m-ZrO_2 and t-ZrO_2 phases has been attributed to the higher concentration of anionic defects on m-ZrO_2 than t-ZrO_2 [42,43].

Within this context, we studied the CPO of methane over Rh/ZrO_2 systems, at different Rh loading, by using m-ZrO_2 or t-ZrO_2 as support. Catalysts were characterized by X-ray diffraction (XRD), BET area determination, X-ray photoelectron spectroscopy (XPS), Fourier transformed infrared (FTIR) spectroscopy with probe molecules, and H_2/O_2 titration to determine textural features of the supports and the nature of supported Rh species (dispersion, oxidation state, coordinative vacancies). Results on characterization and catalytic activity are presented and discussed, focusing on the influence of Rh loading, Rh particle dimensions and ZrO_2 crystallographic modifications.

2. Experimental

2.1. Samples preparation

Two procedures were adopted to prepare the ZrO_2 support. The first procedure involved the precipitation of hydrous zirconium oxide by bubbling a stream of ammonia-saturated N_2 into a $ZrOCl_2$ solution for 12 h. After separation, the solid was washed (negative test of Cl^- in the solid), dried at 383 K for 24 h and subsequently heated at 1173 K for 7 h in air [46]. In the second procedure, after precipitation of hydrous zirconium oxide by bubbling a stream of ammonia-saturated N_2 into a $ZrOCl_2$ solution for 12 h, the slurry was kept under reflux at 373 K and 1 atm for 240 h [41], while maintaining the pH at 10. Subsequently, after separation, the solid was washed (negative test of Cl^- in the solid), dried at 383 K for 24 h and then heated at 1173 K for 7 h in air. The resulting zirconium oxides, according to X-ray analysis (see below), were designated as m-ZrO_2 and t-ZrO_2, respectively.

The Rh/ZrO_2 samples were prepared by dry impregnation of m-ZrO_2 or t-ZrO_2 solids with the appropriate amount of a $Rh(NO_3)_3$ standardized aqueous solution to have samples with various rhodium content (0.04–3.3 wt%), followed by drying at 383 K for 12 h in air (*as prepared* samples).

Samples were indicated as *y*-ZRh*x*, where *x* stands for the rhodium content, expressed as metal wt% and *y* stands for the ZrO_2 crystalline tetragonal (t) or monoclinic (m) modification.

2.2. Characterization

X-ray diffraction (XRD) patterns in the 2θ angular range from 5 to 60° were obtained with a Philips PW 1729 diffractometer using Cu Kα (Ni-filtered) radiation. The volume fraction of tetragonal zirconia, v_t, was obtained with the formula proposed by Toraya et al. [47], as described elsewhere [48].

Surface areas of hydrous zirconium oxides, m-ZrO_2 and t-ZrO_2 were determined by N_2 adsorption at 77 K (BET method) using a Micromeritics ASAP 2010 apparatus. Before the measurement, samples were outgassed for 2 h at 473 K.

XPS measurements were made on a Leybold-Heraeus LHS10 spectrometer operating in FAT mode (50 eV pass energy) with Al Kα radiation source (12 kV/20 mA) at a pressure lower than 10^{-7} Pa. The *as prepared* samples, meshed to fine powders (<106 μm), were manually pressed onto a gold plate attached to the sample rod. Reduction treatments in situ in a flowing H_2/N_2 mixture (H_2 10%, 6 mL/min) in the temperature range 623–693 K for 1 h were carried out in a chamber connected to the preparation chamber. The treatment temperatures refer to the effective sample temperature monitored by a thermocouple contacting the sample surface. After being cooled gradually to room temperature in the H_2/N_2 stream the sample was transferred in vacuum to the preparation chamber and then pushed into the analysis chamber for spectra collection. The Rh(3d), C(1s), O(1s) and Zr(3d) regions were sequentially acquired. Binding energy (BE) values were referenced to Zr($3d_{5/2}$) at 182.5 eV and measured with an accuracy of ±0.2 eV. Data analysis involved non-linear Shirley-type background subtraction and curve-fitting by Esca Tools 4.2 software (Surface Interface Inc., Mountain View, CA). Changes in Rh(3d) signal shape on reduced samples were analyzed by curve-fitting procedures with Rh(3d) doublets endowed with fixed spectroscopic parameters (Rh($3d_{5/2}$–$3d_{3/2}$) spin–orbit separation, 4.8 eV and intensity ratio $R = 0.66$) but using variable position, full width at half maximum (FWHM) and intensities.

Rh dispersion, defined as the ratio of the exposed Rh atoms (Rh_{exp}) to the number of total Rh atoms (Rh_{tot}), was determined by H_2/O_2 titration [49] using a volumetric apparatus. The *as prepared* samples (0.5–2 g, depending on Rh content) were pre-treated in flowing N_2 at 423 K for 30 min, reduced in H_2 (10% in He) at 773 K for 1 h and then purged with N_2 at 773 K for 1 h before cooling down to RT in N_2. In selected cases, the reduction temperature was 623 K. Samples were then exposed to O_2 (10% in N_2) at RT for 30 min, flushed with N_2 for 30 min at RT. After evacuation at RT down to 1 Pa, the irreversibly adsorbed H_2 at RT, H_{irr}, was determined by the double isotherm method. First, total H_2 uptake was determined by zero pressure extrapolation of the adsorption isotherm, usually in the pressure range 6.6–26.6 kPa. Samples were subsequently evacuated at RT for 0.5 h and a second isotherm due to the reversible part of the adsorption was determined. The difference between the total (first isotherm) and the reversible (second isotherm) uptakes in the parallel and linear part of the isotherms gave the irreversible part of the hydrogen adsorption, H_{irr}. The exposed Rh atoms (Table 1) were calculated from H_{irr}, assuming H_{irr}/Rh_{exp} ratio of 1 and by taking into account the overall stoichiometry: $Rh_{exp}\text{-}O + 3/2H_2 = Rh_{exp} - H_{irr} + H_2O$. The Rh dispersion, D, was then calculated as H_{irr}/Rh_{tot}. The mean Rh particle size, d, was calculated assuming spherical geometry, $d = 6(v_m/a_m)/D$, where a_m and v_m are the effective average area occupied by a metal atom on the surface (Rh, 7.58 Å^2) and the volume per metal atom in the bulk (Rh, 13.78 Å^3), respectively [50]. For some representative samples, Rh dispersion, D, and mean Rh particle size, d, were calculated on samples *aged* under catalytic conditions (see below) at 1023 K and then treated in O_2 at 773 K.

IR spectra were run at room temperature (RT) on an FTIR spectrometer (Perkin Elmer 2000), equipped with a MCT detector, operating at a resolution of 4 cm^{-1}. The *as prepared* samples were pelletted (pressure of 2×10^4 kg cm^{-2}) in self-supporting disks of ca. 13 mg cm^{-2}, and introduced into a cell which allowed thermal treatments in vacuum or in a controlled atmosphere. CO adsorption (99.9%, Rivoira) at RT was conducted on samples heated in O_2

Table 1
Catalysts and their main features.

Catalyst[a]	D[b]	D_{aged} [c]	d[b]/nm	d_{aged} [c]/nm	$[Rh_{exp}]$[d]/(10^{18} atoms g^{-1})	$[Rh_{exp}]_{aged}$ [e]/(10^{18} atoms g^{-1})
t-ZRh0.04	0.94	–	1.16	–	2.30	–
t-ZRh0.10	0.76	–	1.43	–	4.60	–
t-ZRh0.19	0.64	0.35	1.70	3.12	7.11	3.89
t-ZRh0.50	0.72	0.63	1.51	1.73	21.1	18.4
t-ZRh1.0	0.50	–	2.18	–	29.3	–
t-ZRh2.0	0.42	0.30	2.60	3.64	49.2	35.1
t-ZRh3.3	0.25	–	4.36	–	51.5	–
m-ZRh0.10	0.82	–	1.33	–	4.80	–
m-ZRh0.25	0.38	–	2.87	–	5.60	–
m-ZRh0.39	0.28	0.16	3.90	6.82	6.39	3.65

[a] BET surface area was 22 $m^2 g^{-1}$ for t-ZrO_2 support and 6 $m^2 g^{-1}$ for m-ZrO_2.
[b] Rh dispersion (D), and mean diameter of Rh particles (d), calculated by H_2/O_2 titration, on samples reduced in H_2 at 773 K.
[c] Rh dispersion and mean diameter of Rh particles calculated on samples aged in catalytic conditions at 1023 K and then treated in O_2 at 773 K.
[d] Exposed Rh atoms *per* gram of catalyst on samples reduced in H_2 at 773 K.
[e] Exposed Rh atoms *per* gram of catalyst on samples aged in catalytic conditions at 1023 K and then treated in O_2 at 773 K.

(1.33×10^4 Pa; SOL 99.5%) at 773 K for 1 h, evacuated at the same temperature for 1 h, exposed to H_2 (1.0×10^4 Pa; Rivoira, 99.9%) at 623 K for 30 min, and evacuated at 773 K for 1 h. Before contacting with samples, all gases were purified in a liquid nitrogen trap.

2.3. Catalytic tests

Catalytic activity was measured in a flow apparatus at atmospheric pressure. The apparatus included a feeding section, independent mass flow controller-meters (MKS mod. 1259, driven by a four-channel unit MKS mod. 647C) and glass ampoule for gas mixing before entering the reactor. High purity gas mixtures (CH_4/N_2, O_2/N_2, H_2/N_2, and N_2; Rivoira) were used without further purification. The fixed bed tubular reactor was made of two coaxial quartz tubes (i.d. 20 and 10 mm) to allow preheating of feed gas. The temperature of the catalytic bed was monitored by a K-type thermocouple, located in a quartz tube (i.d. 4 mm) concentric to the reactor. Reactants and products were analyzed by a gas-chromatograph (Agilent 7890A GC system), equipped with three columns (Molsieve 5A for detecting O_2 and CO, Porapack Q for CO_2, and Na_2SO_4-doped alumina for H_2 and CH_4) and two detectors (TCD and FID). The *as prepared* catalysts were sieved to 180–250 μm and deposited (about 10 mg) on a ceramic wool in the reactor. Before each run, catalysts were treated in a 5% O_2/N_2 flow at 773 K for 2 h, reduced in 10% H_2/N_2 stream at 623 K for 2 h and purged with N_2 at 623 K for 10 min. The typical catalytic run consisted of measurements at steady-state with a mixture of 2% CH_4, 1% O_2, balance N_2, in the temperature range from 573 to 1023 K. When changing the temperature (in a random sequence) the catalyst was left in contact with the reactant mixture. Space velocity was 9×10^5 NL kg_{cat}^{-1} h^{-1} (contact time $\tau \simeq 2$ ms). To check the catalytic reproducibility three runs were carried out for each catalyst. The stability of the catalysts was tested by following the reaction at 1023 K for 6 h. In some experiments O_2 concentration was changed to 3% or 0.5%. To compare catalytic activity and selectivity of the various catalysts, we assumed the following set of reactions to take place on all catalysts:

$$CH_4 + 1/2O_2 \rightarrow CO + 2H_2 \quad (1)$$

$$CH_4 + 3/2O_2 \rightarrow CO + 2H_2O \quad (2)$$

$$CH_4 + 2O_2 \rightarrow CO_2 + 2H_2O \quad (3)$$

Percent CH_4 conversion was calculated as 100 × (CH_4 molecules consumed)/(CH_4 molecules injected). Percent H_2, CO or CO_2 yields were calculated as 100 × (H_2 molecules produced)/(1/2 CH_4 molecules injected), and 100 × (CO or CO_2 molecules produced)/(CH_4 molecules injected). Selectivity to H_2 was calculated as 100 × (H_2 molecules produced/1/2 CH_4 molecules converted). Selectivity to CO was calculated as 100 × (CO molecules produced/CH_4 molecules converted). Conversions obtained at various (sample weight)/(flow rate) ratios (W/F) indicated that, in our conditions, reaction is under kinetic control without diffusion effect. For each catalyst, reaction rates of H_2 formation, R_{H_2} (R_{H_2}/molecules s^{-1} g^{-1}), were calculated from H_2 yield values not exceeding 30% and far from the thermodynamic equilibrium. Activation energy values (E_a/kJ mol^{-1}) were determined from log R_{H_2} vs $1/T$ plot. The turnover frequency numbers, N_{H_2} (N/molecules s^{-1} $atom^{-1}$) were calculated as $N_{H_2} = R_{H_2}/[Rh_{exp}]$, where $[Rh_{exp}]$ ($[Rh_{exp}]$/atoms g^{-1}) is the concentration of exposed Rh atoms determined by H_2/O_2 titration on samples *aged* under catalytic conditions.

3. Results and discussion

3.1. Structural and textural properties of catalysts

After calcination at 1173 K for 7 h, the crystal phase of the zirconia obtained from the precipitated hydrous zirconium oxide was purely monoclinic (m-ZrO_2). On the contrary, ZrO_2 resulting from calcination at 1173 K for 7 h of the precursor obtained by precipitation and refluxing for 240 h was predominantly tetragonal (t-ZrO_2). The tetragonal volume fraction, v_t, resulted 0.92.

The X-ray diffraction patterns of all the Rh containing samples before and after catalytic tests revealed no changes in the relative amounts of the ZrO_2 monoclinic and tetragonal modification, and no lines due to metal Rh, which implies that Rh was highly dispersed on the sample surface as nanoparticles.

The effects of preparation method and calcination temperature appeared also on the surface area of zirconia. After drying at 383 K hydrous zirconium oxide prepared by the reflux method exhibited a BET surface area (480 $m^2 g^{-1}$) much higher than that of the precursor prepared by precipitation (330 $m^2 g^{-1}$). The difference in surface area values was retained after thermal treatment at 1173 K: a surface area of 22 $m^2 g^{-1}$ was measured for the t-ZrO_2, whereas a value of 6.0 $m^2 g^{-1}$ was obtained for the m-ZrO_2. The structural and textural properties of the zirconia supports are consistent with those reported in studies concerning the effects of synthesis and calcination conditions on the bulk and surface properties of ZrO_2 [41].

The Rh dispersion, D, obtained on samples reduced in H_2 at 773 K, depends both on the metal loading and on the support crystalline phase. The dispersion decreased with increasing Rh loading on both supports (Table 1), the t-ZrO_2 support giving higher dispersion than m-ZrO_2. For t-ZRhx samples, at increasing metal loading,

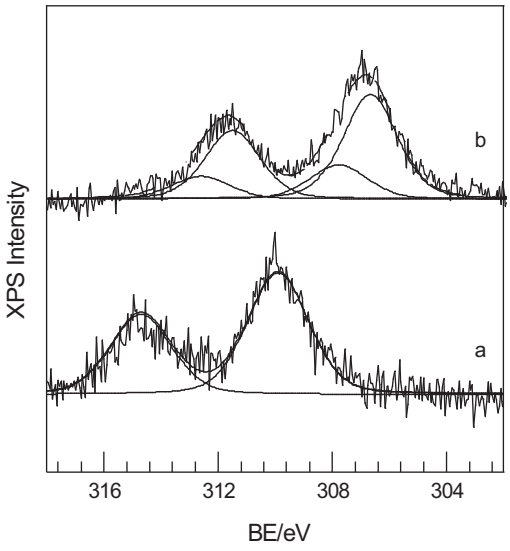

Fig. 1. Rh3d XPS peaks recorded on t-ZRh1.0. Section a: *as prepared* sample; section b: after in situ reduction at 673 K 1 h with curve fitting components.

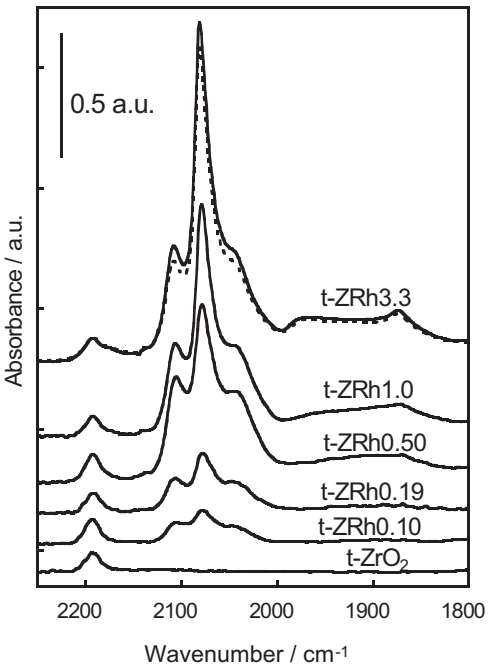

Fig. 2. FTIR spectra of CO adsorbed at RT (equilibrium $P_{CO} = 1.33 \times 10^4$ Pa) on t-ZRhx samples reduced at 623 K (solid lines) or 773 K (dotted line).

dispersion remained fairly constant up to $x = 0.50$ wt% ($D = 0.72$) and then markedly decreased, approaching a limit value of 0.25 for $x = 3.3$ wt%. Conversely, for m-ZRhx samples, Rh dispersion decreased rapidly from 0.82 to 0.28 by varying Rh loading from 0.10 to 0.39 wt%. In all cases, dispersion data indicated the presence of small metal nanoparticles having mean diameter varying in the $1.16 \leq d \leq 4.36$ nm range (Table 1), whose dimension increased with Rh content.

The influence of the reduction temperature (623 K vs 773 K) on Rh dispersion was evaluated on the t-ZRh3.3 and m-ZRh0.39 samples. While no appreciable difference in the Rh dispersion was found for the t-ZRh3.3 sample (0.26 at 623 K vs 0.25 at 773 K), a great difference was revealed on the m-ZRh0.39 sample (0.46 at 623 K vs 0.28 at 773 K). These findings clearly indicate that the interaction of the Rh particles with the t-ZrO_2 surface is stronger than that with the m-ZrO_2 one.

To check whether the oxidation pre-treatment of the samples adopted for the catalytic tests (5% O_2/N_2, flow at 773 K for 2 h) had any effect on Rh sintering, Rh dispersion was determined on the t-ZRh0.50 sample pre-treated in O_2 at 773 K. A value similar to that obtained on the t-ZRh0.50 sample exposed to conventional H_2/O_2 titration was found within the experimental error (±5%) (Table 1).

The effect of aging time on metal dispersion was also considered. Treatments at 1023 K for 6 h in catalytic conditions yielded a decrease in the metal dispersion, *D*, in both set of samples (Table 1). A strong effect was apparent for the m-ZRh0.39 sample (0.28 vs 0.16), whereas for the t-ZRhx system it was progressively less marked at increasing Rh content (0.64 vs 0.35 for t-ZRh0.19; 0.72 vs 0.63 for t-ZRh0.50 and 0.42 vs 0.30 for t-ZRh2.0).

XPS analysis of both t-ZRhx and m-ZRhx *as prepared* samples showed practically constant $Rh3d_{5/2}$ BE values at 309.6 ± 0.2 eV (FWHM in the range 2.4–2.7 eV) corresponding to Rh^{3+} state [51].

The evolution of the surface state of rhodium species was investigated performing in situ treatments in the H_2/N_2 mixture at 673 K for 1 h. Rh3d spectra collected before and after hydrogen treatments are shown in Fig. 1(curves a and b, respectively) for the t-ZRh1.0 sample, as a representative case. Reduction treatment at 673 K for 1 h yielded an asymmetric peak broadening and shift to a lower BE, suggesting the presence of rhodium species with wide cluster size distribution and/or different oxidation state. The $Rh3d_{5/2}$ component resulted at 307.0 eV, a value slightly higher than that of rhodium in the metallic state [51]. The asymmetric Rh3d region was satisfactorily reproduced by curve fitting with two components at 306.7 eV and 307.5 eV, respectively (Fig. 1b). The component at 306.7 eV indicates the presence of rhodium in the metallic state, whereas the one at 307.5 eV can be attributed to positively charged small rhodium species, $Rh^{\delta+}$, rather than to rhodium species in a specific oxidized form. Small positive BE shifts have also been observed with other catalytic systems and attributed to changes in the metal cluster size [52–54]. The increase in the measured binding energy, interpreted as final state effect [55], indicates a reduced screening of the photoelectron core hole on the final-state electron due to the small cluster size.

The Rh3d/Zr3d intensity ratios, measured for *as prepared* and H_2-treated (623 K) t-ZRhx samples with Rh content from 0.50 to 3.3 wt%, matched fairly well those predicted assuming a uniform spreading of the rhodium species on the ZrO_2 surface [56], thus confirming the persistence of rhodium particles in a dispersed state.

FTIR of adsorbed CO has been applied to identify the nature of Rh surface sites because distinct adsorption bands originate from the interaction of CO with various Rh surface species [57].

Exposing t-ZRhx samples reduced at 623 K to CO at RT resulted with a band at about 2195 cm^{-1} due to the Zr^{4+}-CO species [58] and bands in the region 2100–1850 cm^{-1}, assignable to linear and bridged CO species adsorbed on Rh particles [59–63]. In particular, CO adsorption yielded linear Rh^0-CO carbonyl on Rh^0 in nanoparticles (2075 cm^{-1}) [59–63], Rh^+-$(CO)_2$ dicarbonyls (ν_{sym} and ν_{asym} at 2105 and 2042 cm^{-1}) arising from oxidation of isolated Rh^0 or Rh^0 in very small clusters [60,61,64], and bridged $Rh^0{}_x(CO)_y$ species (broad band at about 1950–1850 cm^{-1}) formed on Rh^0 in extended particles [59,60], the latter detected on samples with $x > 0.50$ wt% ($d > 1.5$ nm) (Fig. 2, solid spectra). The overall intensity of the carbonyl bands increased in parallel with the amount of exposed Rh in the samples (compare spectra in Fig. 2 and data in Table 1). The presence of a high amount of Rh^+-$(CO)_2$ even in the t-ZRh3.3 sample, in which a high amount of Rh^0 isolated or in very small clusters is not likely to be present, suggests that Rh^0 sites yielding Rh^+ are the less-coordinated Rh atoms at the boundary of metal particles. These border Rh atoms interact with the t-ZrO_2

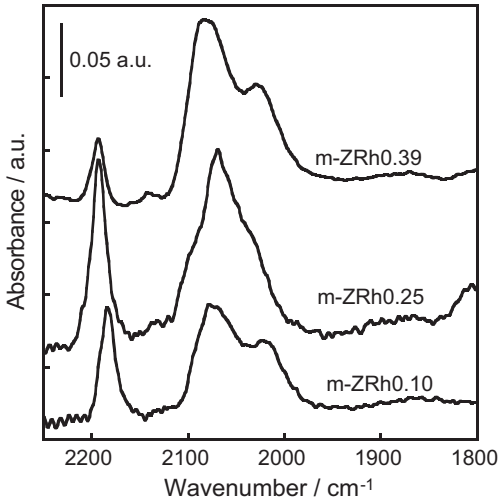

Fig. 3. FTIR spectra of CO adsorbed at RT on m-ZRhx samples reduced ad 623 K (equilibrium $P_{CO} = 1.33 \times 10^4$ Pa).

support and therefore possess a lower metal character than those located in the bulk of Rh particles.

The occurrence of Rh-carbonyl bands at the same positions on all t-ZRhx samples suggests the presence of exposed Rh sites of the same type, whose relative amount somewhat depends on Rh content. In fact, as the Rh loading increased, both the intensity ratio Rh^0-CO/Rh^+-$(CO)_2$ and the intensity of the $Rh^0_x(CO)_y$ band increased, indicating an increase of particle mean dimension, in agreement with H_2/O_2 titration findings (Table 1).

Raising the reduction temperature from 623 to 773 K, t-ZRhx samples yielded the same Rh-carbonyl species with a slightly lower intensity (about 10%, from integrated area in the range 2160–1725 cm^{-1}). This result shows the stability of Rh particles on t-ZrO_2 up to 773 K. As an example, the spectrum of the t-ZRh3.3 sample reduced at 773 K (Fig. 2, dotted line) is compared with that of the same sample reduced at 623 K (solid line).

On m-ZRhx samples, pre-reduced at 623 K, CO adsorption at RT yielded, in addition to the band typical of m-ZrO_2 due to Zr^{4+}-CO species (~2190–2200 cm^{-1}) [65], an unresolved absorption band in the range 2000–2120 cm^{-1} ascribed to linear Rh^0-CO and to a small amount of Rh^+-$(CO)_2$ species (Fig. 3). Bands of carbonates (1550, 1305, and 1060 cm^{-1}) and bi-carbonates (1630, 1420, and 1220 cm^{-1}) [66,67] (spectral region not shown), arising from adsorption of CO_2 produced in the Boudouard equilibrium, were also recorded, as already observed on similar Rh/m-ZrO_2 systems [59,68]. The overall Rh-carbonyl intensity was nearly the same in the three monoclinic samples, in agreement with the fact that they exposed a similar amount of Rh atoms (see Table 1).

Comparing CO adsorption on tetragonal and monoclinic samples with Rh particle having similar mean diameter (i.e. similar dispersion, see Table 1), m-ZRh0.10 vs t-ZRh0.10 (Fig. 4a) and m-ZRh0.39 vs t-ZRh3.3 samples (Fig. 4b), we observed that (i) Rh^0-CO band was narrower and (ii) Rh^+-$(CO)_2$ bands were more intense on the t-ZRhx samples than on the m-ZRhx ones. The first evidence reveals that Rh^0 sites with a strong metal character were more homogeneous (i.e. with similar near-neighbor atoms) in the t-ZRhx samples than in the m-ZRhx ones. The second fact indicates that Rh sites with a lower metal character (i.e. those interacting with the support) were more abundant on tetragonal than on monoclinic zirconia, thus suggesting a stronger interaction of Rh species with the surface of the tetragonal with respect to the monoclinic support. A possible explanation of this finding could be found in the more covalent character of the Zr–O bond and more oxygen defective structure of m-ZrO_2 with respect to t-ZrO_2 [43,69] which could cause a more difficult electron transfer from Rh^0 species to the m-ZrO_2 surface with a consequent weakening of the surface-Rh interactions.

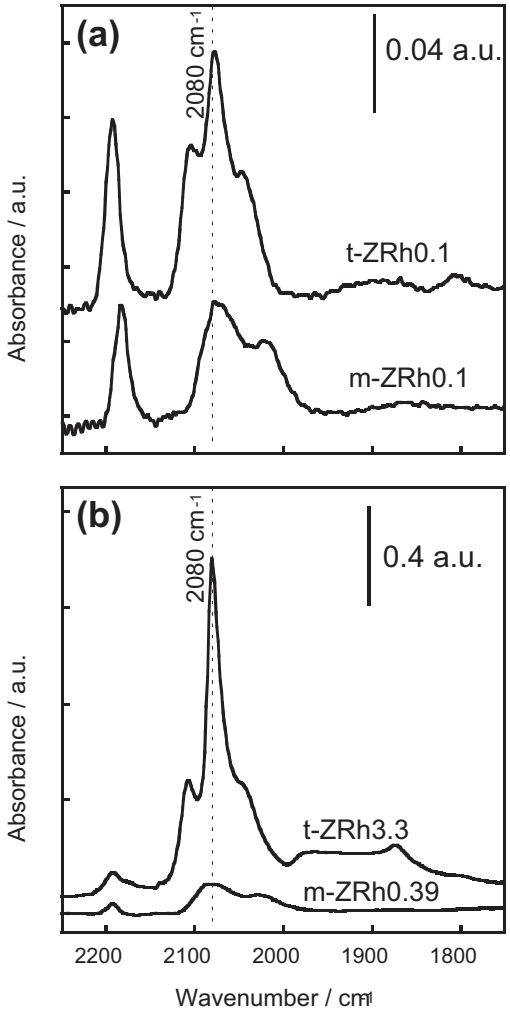

Fig. 4. Comparison of CO adsorbed species (equilibrium $P_{CO} = 1.33 \times 10^4$ Pa) on t- and m-ZRhx samples with particles having similar mean diameter. Samples with 1.3 and 1.4 nm of diameter (section a) or 4.3 and 3.9 nm of diameter (section b).

3.2. Catalytic properties

3.2.1. The dependence of the catalytic activity on the feed composition

To obtain the best H_2 yield, we first studied the dependence of catalytic activity and selectivity on feed composition in the 673–1023 K temperature range, using the t-ZRh0.50 sample as a reference (Fig. 5). Tests with feed composition $CH_4/O_2 = 0.66$ (Fig. 5a) gave CH_4 conversion of 20–90%, CO_2 and H_2O as main products and very low (≤27%) H_2 yield showing that methane total oxidation to CO_2, reaction (3), prevailed on partial oxidation, reaction (1).

With the mixture $CH_4/O_2 = 2$ (Fig. 5b), in the temperature range 673–723 K, the CH_4 conversion was 15–27%, and the only products were CO_2 and H_2O. In the temperature range 723–1023 K, in addition to CO_2 and H_2O, CO and H_2 formed with a molar ratio $H_2/CO = 2$, indicating that in these conditions reactions (1) and (3) occurred. At 1023 K, both the CH_4 conversion and the H_2 yield were above 90% (Fig. 5b).

Gas mixture with $CH_4/O_2 = 4$ (Fig. 5c) yielded CH_4 conversion of 18–48% and CO and H_2 as products. At 1023 K, the H_2 yield was 48%.

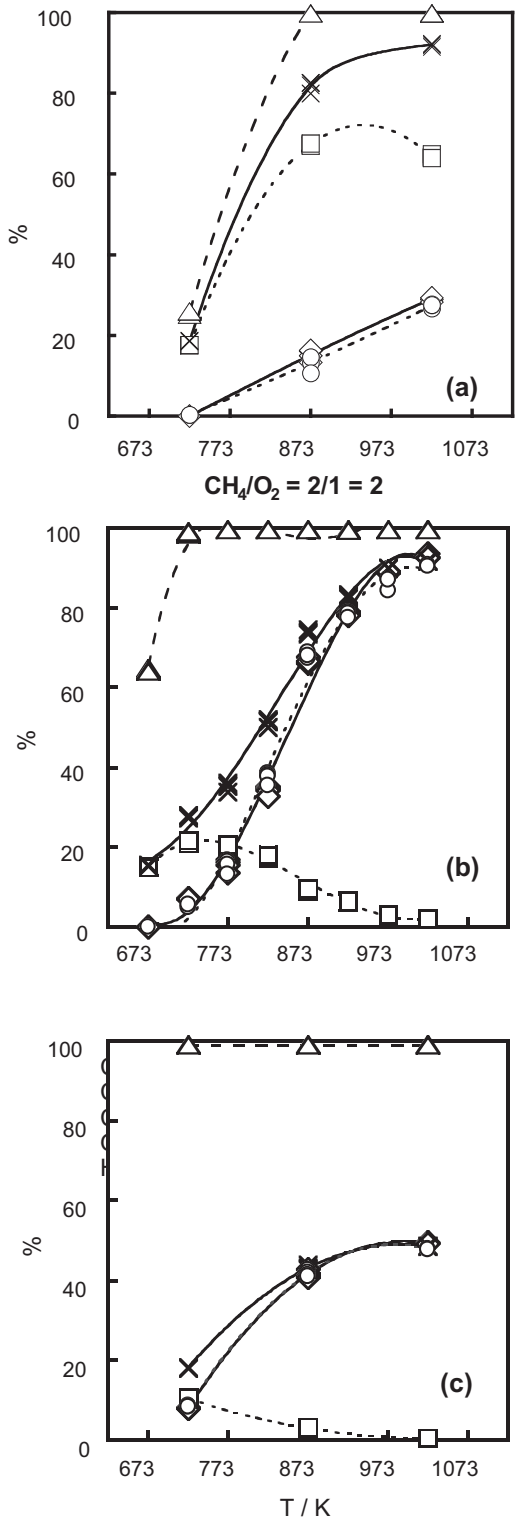

Fig. 5. Dependence of activity on the CH_4/O_2 ratio in the reactant mixture: (×) CH_4 conversion, (△) O_2 conversion, (◊) CO yield, (□) CO_2 yield and (○) H_2 yield as a function of temperature. Catalyst: t-ZRh0.50. Section a: $[CH_4] = 2\%$, $[O_2] = 3\%$. Section b: $[CH_4] = 2\%$, $[O_2] = 1\%$. Section c: $[CH_4] = 2\%$, $[O_2] = 0.5\%$.

Notwithstanding only the partial oxidation occurred, reaction (1), the CH_4 conversion was markedly lower than that obtained with the mixture $CH_4/O_2 = 2$.

These results prompted us to perform catalytic experiments with a mixture containing CH_4 and O_2 in the ratio of 2.

3.2.2. The catalytic activity of t-ZRhx samples

In the 573–1023 K temperature range, all t-ZRhx catalysts were active for the CPO of methane, whereas the t-ZrO_2 support was inactive up to 1023 K. As already reported by Bruno et al. [12] and by Beretta et al. [70], three successive runs were always necessary to obtain the highest catalytic activity level. In detail, in the 573–1023 K range, on all t-ZRhx catalysts, CH_4 conversion, H_2 yield and selectivities to CO and H_2 increased with temperature (Fig. 6a–d). For all the samples, below 923 K, CO selectivity was lower than 100% (Fig. 6c), showing that also the total oxidation of methane, reaction (3), occurred.

As the Rh content increased from 0.04 wt% to 0.50 wt%, CH_4 conversion, H_2 yield and selectivities to H_2 and CO markedly increased. On these samples, in the whole temperature range, the H_2 selectivity was lower than 100% and the H_2/CO molar ratio was lower than 2, indicating that the reaction $CH_4 + 3/2O_2 \rightarrow CO + 2H_2O$ (2) was also occurring. At higher Rh content ($x \geq 0.50$ wt%), CH_4 conversion (Fig. 6a), H_2 yield (Fig. 6b) and selectivities to CO (Fig. 6c) and H_2 (Fig. 6d) increased with temperature up to 873 K. At higher temperature, CH_4 conversion approached the equilibrium values (Fig. 6a, dotted line), and CO and H_2 selectivities approached the 100% value (Fig. 6c and d). In particular, at a temperature higher than 823 K, the molar ratio H_2/CO was about 2, indicating that the CPO reaction was prevalent.

The catalyst stability, as a function of time on stream, was tested throughout experiments lasting up to about 6 h at 1023 K (Fig. 7). Catalysts with a Rh content $x \geq 0.50$ wt% were stable. Catalysts with $x < 0.50$ wt% progressively deactivated, probably due to the sintering of Rh particles.

The activation energy values for the CPO reaction were $E_a = 140 \pm 20$ kJ mol^{-1} for samples with a Rh content $x < 0.50$ wt%, and $E_a = 85 \pm 10$ kJ mol^{-1} for the more concentrated t-ZRhx samples ($x \geq 0.50$ wt%), suggesting that the nature of active site somewhat differed in the two concentration regions.

3.2.3. The catalytic activity of m-ZRhx samples

The m-ZrO_2 support was completely inactive for the methane CPO reaction up to 1023 K. The m-ZRhx samples with $x = 0.10$ and 0.25 Rh wt% were also nearly inactive, the H_2 yield being ≤5% in the whole temperature range (Fig. 8a). The m-ZRh0.39 sample showed a low activity starting from 773 K, the H_2 yield being ≤12% up to 1023 K (Fig. 8a). For all the m-ZRhx catalysts, in the 773–1023 K temperature range, the selectivities to CO and H_2 (Fig. 8b) increased with temperature. In particular, for m-ZRh0.39, the maximum selectivity to CO was 65% and the maximum selectivity to H_2 was 35%, indicating that, besides CPO (reaction (1)), both the total oxidation of methane, $CH_4 + 2O_2 \rightarrow CO_2 + 2H_2O$ (3), and the reaction $CH_4 + 3/2O_2 \rightarrow CO + 2H_2O$ (2) occurred.

The m-ZRh0.39 catalyst was stable, as a function of time on stream, throughout experiments lasting up to about 6 h at 1023 K (Fig. 7). On this sample, the activation energy value for the CPO reaction was $E_a = 87 \pm 10$ kJ mol^{-1}.

3.2.4. The dependence of Rh catalytic activity on the support

The CPO catalytic activity and selectivity were higher on t-ZRhx catalysts than on m-ZRhx ones, showing a beneficial effect of the ZrO_2 tetragonal phase (see Fig. 6 vs Fig. 8). As the Rh dispersion was higher on t-ZrO_2 than on m-ZrO_2 (H_2/O_2 titration evidence), possibly due to stronger Rh-support interaction (FTIR evidence), these results suggest a role of dispersion in determining the activity. To clarify this aspect, we compared the activity of t-ZRh0.50 with that of m-ZRh0.39. Having similar E_a values ($E_a = 96$ and 87 kJ mol^{-1} on t-ZRh0.50 and m-ZRh0.39, respectively), the activity order of their supported Rh species could be assessed by comparing the turnover frequency numbers, N_{H_2} (N/molecules s^{-1} atom^{-1}) (Fig. 9). These values were calculated as $N_{H_2} = R_{H_2}/[Rh_{exp}]$, where R_{H_2} is the rate

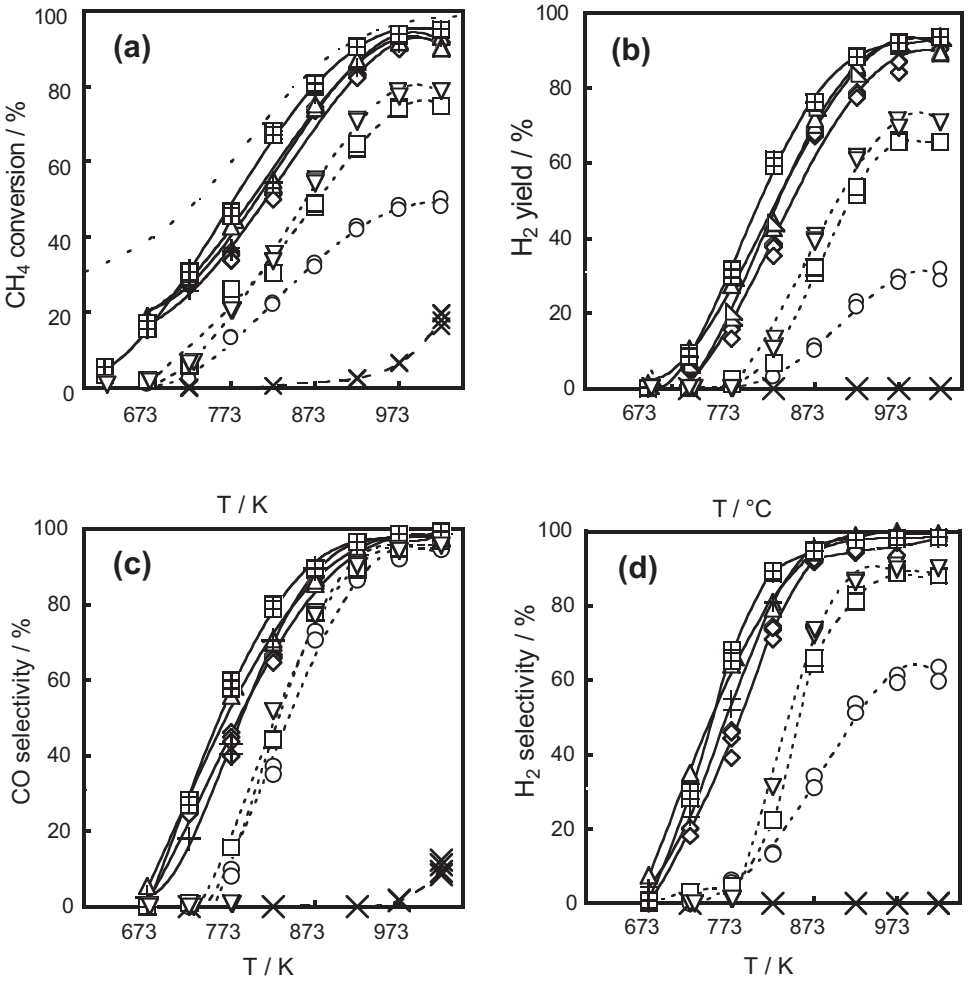

Fig. 6. Catalytic activity and selectivity on t-ZRhx catalysts as a function of temperature. CH_4 conversion (section a), H_2 yield (section b), selectivity to CO (section c), and selectivity to H_2 (section d) on (×) t-ZrO_2, (○) t-ZRh0.04, (□) t-ZRh0.1, (▽)t-ZRh0.19, (◊) t-ZRh0.5, (△) ZRh1, (+) ZRh2.0, (⊞) t-ZRh3.3 catalysts, and calculated at the thermodynamic equilibrium (- - -).

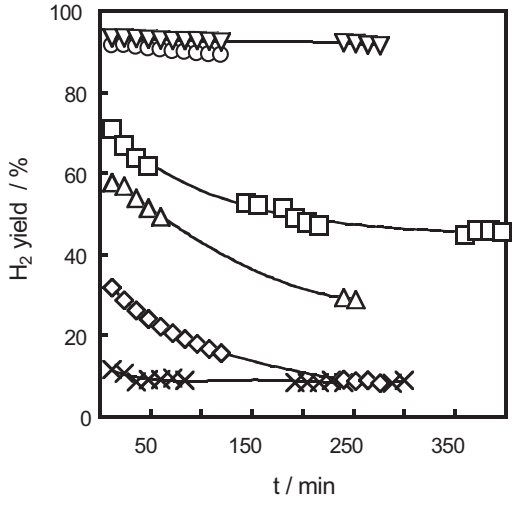

Fig. 7. H_2 yield vs time on stream on t- and m-ZRhx samples. Methane CPO reaction at 1023 K. Catalysts: (◊) t-ZRh0.04, (△) t-ZRh0.10, (□) t-ZRh0.19, (○) t-ZRh0.50, (▽) t-ZRh3.3, and (×) m-ZRh0.39.

of H_2 formation (R_{H_2}/molecules s^{-1} g^{-1}), and [Rh_{exp}] is the concentration of exposed Rh atoms on aged samples ([Rh_{exp}]/atoms g^{-1}), namely Rh atoms effectively exposed under reaction conditions. Because the calculation assumes that all these exposed Rh atoms are active sites, the N_{H_2} values should be regarded as a lower limit. The comparison showed that exposed Rh species on t-ZRh0.50 catalyst were about 3 times more active than exposed Rh species on m-ZRh0.39 one. As the calculation of the N_{H_2} values takes into account only Rh atoms exposed on the surface of the aged samples, the stronger interaction of Rh species with the tetragonal than with the monoclinic ZrO_2 surface (i.e. the higher Rh dispersion on the tetragonal than on the monoclinic ZrO_2 surface) cannot be the only factor responsible for the better catalytic performances of the t-ZRhx samples. As a matter of fact, all t-ZRhx catalysts needed at least three subsequent catalytic runs to reach a stable behavior, with progressive increase in H_2 and CO yields, whereas the m-ZRh0.39 catalyst was stable from the first run. These results could indicate that highly dispersed Rh species, initially present on the surface of all t-ZRhx samples, were not suitable for good catalytic performances. As already discussed for Rh/ZrO_2 [12] and Rh/Al_2O_3 [12,70] catalysts, subsequent catalytic runs induced a surface reconstruction leading to the formation of large metal particles (probably not exceeding 4 nm in mean diameter) with a consequent enhancement of the catalytic activity. Therefore, the higher activity of t-ZRhx samples with respect to m-ZRhx ones could arise from the

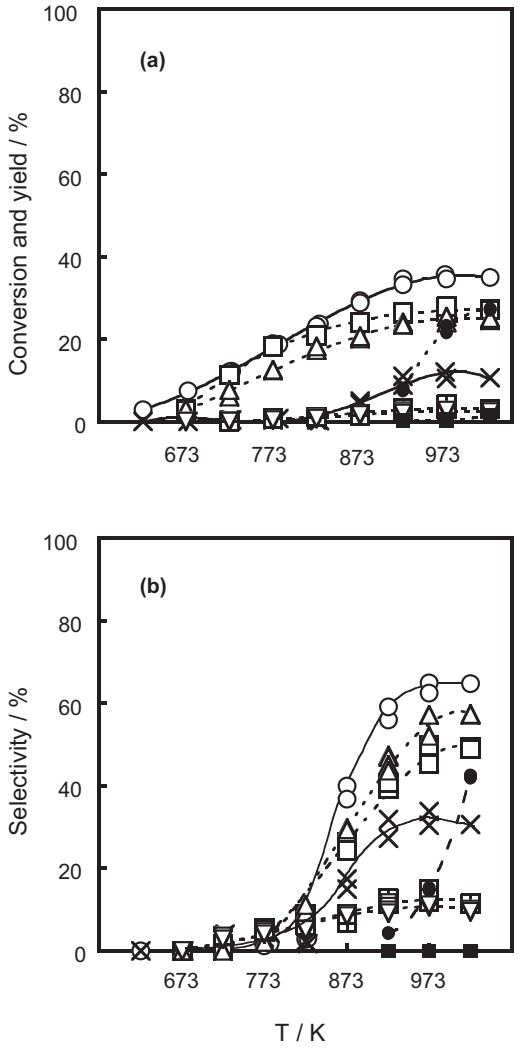

Fig. 8. Catalytic activity and selectivity on m-ZRhx catalysts as a function of temperature. Section a: CH_4 conversion (first symbol), and H_2 yield (second symbol). Section b: selectivity to CO (first symbol), and to H_2 (second symbol). Catalysts: (□, ⊞) m-ZRh0.10; (△,▽) m-ZRh0.25; (○,×) m-ZRh0.39; (●,■) m-ZrO_2.

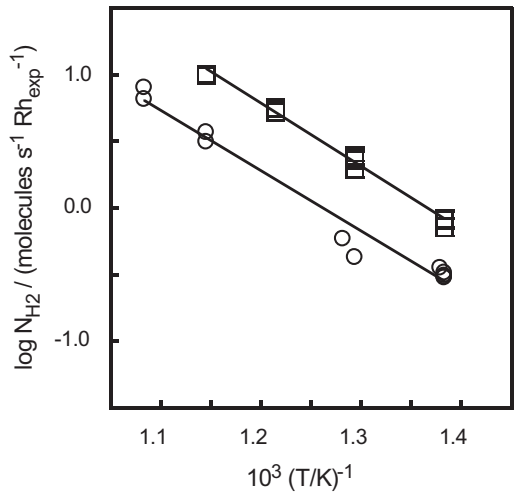

Fig. 9. Turnover frequency *per* exposed Rh atom (N_{H_2}/molecules s^{-1} $Rh_{exp}{}^{-1}$) on (□) t-ZRh0.50 and (○) m-ZRh0.39 catalysts.

higher homogeneity of Rh^0 sites, i.e. from the presence of a higher amount of Rh^0 species with similar near-neighbor atoms.

4. Conclusions

An important role of the support emerges from the study of the catalytic partial oxidation (CPO) of methane on Rh/ZrO_2 catalysts.

Catalytic results show that t-ZRhx catalysts are far more active and selective than m-ZRhx ones.

Characterization results show that the nature of supported Rh species strongly depends on the support. With respect to m-ZrO_2, on t-ZrO_2 samples Rh^0 species are more homogeneous, i.e. with similar near-neighbor atoms (FTIR evidence), more dispersed (H_2/O_2 titration evidence), and their interaction with the support is stronger (FTIR evidence). We suggest that the weaker interaction of Rh species with the surface of the monoclinic with respect to the tetragonal support is due to the more covalent character of the Zr–O bond and more oxygen defective structure of m-ZrO_2.

The comparison between the turnover frequency numbers, N_{H_2}, of the aged t-ZRh0.50 and m-ZRh0.39 samples suggests that the different strength of interaction of Rh particles with the surface of tetragonal or monoclinic zirconia, responsible for the different dispersion, cannot provide the only explanation for the different catalytic performances of the t-ZRhx and m-ZRhx samples. The higher activity of t-ZRhx samples with respect to m-ZRhx ones could arise also from the presence, in t-ZRhx samples, of a higher amount of Rh^0 species with similar near-neighbor atoms in metal particles not exceeding 4 nm in mean diameter.

Acknowledgment

MIUR-Rome is gratefully acknowledged for financial support.

References

[1] A.P.E. York, T. Xiao, M.L.H. Green, Topics in Catalysis 22 (2003) 345–358.
[2] B.C. Enger, R. Lødeng, A. Holmen, Applied Catalysis A: General 346 (2008) 1–27.
[3] A. Holmen, Catalysis Today 142 (2009) 2–8.
[4] S. Freni, G. Calogero, S. Cavallaro, Journal of Power Sources 87 (2000) 28–38.
[5] D.A. Hickman, L.D. Schmidt, Journal of Catalysis 138 (1992) 267–282.
[6] D.A. Hickman, E.A. Haupfear, L.D. Schmidt, Catalysis Letters 17 (1993) 223–237.
[7] P.M. Torniainen, X. Chu, L.D. Schmidt, Journal of Catalysis 146 (1994) 1–10.
[8] K.L. Hohn, L.D. Schmidt, Applied Catalysis A: General 211 (2001) 53–68.
[9] C.A. Leclerc, J.M. Redenius, L.D. Schmidt, Catalysis Letters 79 (2002) 39–44.
[10] L. Basini, K. Aasberg-Petersen, A. Guarinoni, M. Østberg, Catalysis Today 64 (2001) 9–20.
[11] F. Basile, G. Fornasari, M. Gazzano, A. Kiennemann, A. Vaccari, Journal of Catalysis 217 (2003) 245–252.
[12] T. Bruno, A. Beretta, G. Groppi, M. Roderi, P. Forzatti, Catalysis Today 99 (2005) 89–98.
[13] S. Takenaka, H. Umebayashi, E. Tanabe, H. Matsune, M. Kishida, Journal of Catalysis 245 (2007) 392–400.
[14] B. Kimmerle, A. Baikera, J. Grunwaldtz, Physical Chemistry Chemical Physics 12 (2010) 2288–2291.
[15] S. Rabe, M. Nachtegaal, F. Vogel, Physical Chemistry Chemical Physics 9 (2007) 1461–1468.
[16] S. Eriksson, S. Rojas, M. Boutonnet, J.L.G. Fierro, Applied Catalysis A: General 326 (2007) 8–16.
[17] L. Basini, Catalysis Today 117 (2006) 384–393.
[18] K. Heitnes Hofstad, J.H.B.J. Hoebink, A. Holmen, G.B. Marin, Catalysis Today 40 (1998) 157–170.
[19] P. Aghalayam, Y.K. Park, D.G. Vlachos, Catalysis 15 (2000) 98–137.
[20] V.R. Choudhary, T.V. Choudhary, Angewandte Chemie International Edition 47 (2008) 1828–1847.
[21] V. Dal Santo, C. Mondelli, V. De Grandi, A. Gallo, S. Recchia, L. Sordelli, R. Psaro, Applied Catalysis A: General 346 (2008) 126–133.
[22] Z. Tian, O. Dewaele, G.B. Marin, Catalysis Letters 57 (1999) 9–17.
[23] J. Li, F. Huang, W. Weng, X. Pei, C. Luo, H. Lin, C. Huang, H. Wan, Catalysis Today 131 (2008) 179–187.
[24] M. Zimowska, J.B. Wagner, J. Dziedzic, J. Camra, B. Borzęcka-Prokop, M. Najbar, Chemical Physics Letters 417 (2006) 137–142.
[25] E. Ruckenstein, H.Y. Wang, Journal of Catalysis 187 (1999) 151–159.
[26] S. Hannemann, J. Grunwaldt, B. Kimmerle, A. Baiker, P. Boye, C. Schroer, Topics in Catalysis 52 (2009) 1360–1370.

[27] R. Horn, K.A. Williams, N.J. Degenstein, L.D. Schmidt, Journal of Catalysis 242 (2006) 92–102.
[28] R.C. Ramaswamy, P.A. Ramachandran, M.P. Dudukovic, Industrial & Engineering Chemistry Research 46 (2007) 8638–8651.
[29] J. Wei, E. Iglesia, Journal of Catalysis 225 (2004) 116–127.
[30] A. Beretta, Gi Groppi, M. Lualdi, I. Tavazzi, P. Forzatti, Industrial & Engineering Chemistry Research 48 (2009) 3825–3836.
[31] B.C. Gates, Journal of Molecular Catalysis A: Chemical 163 (2000) 55–65.
[32] A.Yu. Stakheev, L.M. Kustov, Applied Catalysis A: General 188 (1999) 3–35.
[33] K. Hayek, R. Kramer, Z. Paál, Applied Catalysis A: General 162 (1997) 1–15.
[34] C. Jung, Y. Ito, A. Endou, M. Kubo, A. Imamura, P. Selvam, A. Miyamoto, Catalysis Today 87 (2003) 43–50.
[35] B.R. Cuenya, Thin Solid Films 518 (2010) 3127–3150.
[36] Q. Fu, T. Wagner, Surface Science Reports 62 (2007) 431–498.
[37] C.R. Henry, Progress in Surface Science 80 (2005) 92–116.
[38] F. Gao, D.W. Goodman, The Annual Review of Physical Chemistry 63 (2012) 265–286.
[39] K. Tanabe, Materials Chemistry and Physics 13 (1985) 347–364.
[40] G.K. Chuah, S. Jaenicke, Applied Catalysis A: General 163 (1997) 261–273.
[41] K.T. Jung, A.T. Bell, Journal of Molecular Catalysis A: Chemical 163 (2000) 27–42.
[42] K.T. Jung, A.T. Bell, Catalysis Letters 80 (2002) 63–68.
[43] M.D. Rhodes, A.T. Bell, Journal of Catalysis 233 (2005) 198–209.
[44] L. Wang, Q. Liu, M. Chen, Y. Liu, Y. Cao, H. He, K. Fan, The Journal of Physical Chemistry C 111 (2007) 16549–16557.
[45] M. Benito, R. Padilla, L. Rodríguez, J.L. Sanz, L. Daza, Journal of Power Sources 169 (2007) 167–176.
[46] M. Valigi, D. Gazzoli, A. Cimino, E. Proverbio, The Journal of Physical Chemistry B 103 (1999) 11318–11326.
[47] H. Toraya, M. Yoshimura, S. Somiya, Journal of the American Ceramic Society 67 (1984) c119–c121.
[48] D. Gazzoli, S. De Rossi, G. Ferraris, M. Valigi, L. Ferrari, S. Selci, Applied Surface Science 255 (2008) 2012–2019.
[49] J.E. Benson, M. Boudart, Journal of Catalysis 4 (1965) 704–710.
[50] G. Eartl, H. Knözinger, J. Weitkamp (Eds.), Handbook of Heterogeneous Catalysis, vol. 2, Wiley-VCH, Weinheim, 1997, 441 (427–463).
[51] S. Suhonen, R. Pulvinen, M. Valden, K. Kallinen, M. Härkönen, Applied Surface Science 200 (2002) 48–54.
[52] M.G. Mason, Physical Review B 27 (1983) 748–762.
[53] M.Yu. Smirnov, E.I. Vovk, A.V. Kalinkin, A.V. Pashis, V.I. Bukhtiyarov, Kinetics and Catalysis 53 (2012) 117–124.
[54] K. Dohmae, T. Nonaka, Y. Seno, Surface and Interface Analysis 37 (2005) 115–119.
[55] G.K. Wertheim, S.B. Di Cenzo, S.E. Youngquist, Physical Review Letters 51 (1983) 2310–2313.
[56] A. Cimino, D. Gazzoli, M. Valigi, The Journal of Electron Spectroscopy and Related Phenomena 104 (1999) 1–29.
[57] K.I. Hadjiivanov, G.N. Vayssilov, Advances in Catalysis 47 (2002) 307–511.
[58] V. Bolis, G. Cerrato, G. Magnacca, C. Morterra, Thermochimica Acta 312 (1998) 63–77.
[59] E. Finocchio, G. Busca, P. Forzatti, G. Groppi, A. Beretta, Langmuir 23 (2007) 10419–10428.
[60] P. Basu, D. Panayotov, J.T. Yates Jr., Journal of the American Chemical Society 110 (1988) 2074–2081.
[61] H.F.J. Van't Blik, J.B.A.D. van Zon, T. Huizinga, J.C. Vis, D.C. Koningsberger, R. Prins, Journal of the American Chemical Society 107 (1985) 3139–3147.
[62] D.K. Paul, C.D. Marten, Langmuir 15 (1999) 4508–4512.
[63] J.T. Yates Jr., T.M. Duncan, R.W. Vaughan, Journal of Chemical Physics 71 (1979) 3908–3915.
[64] M. Primet, Journal of the Chemical Society, Faraday Transactions 1 (74) (1978) 2570–2580.
[65] C. Morterra, L. Orio, C. Emanuel, Journal of the Chemical Society, Faraday Transactions 86 (1990) 3003–3013.
[66] K. Pokrovski, K.T. Jung, A.T. Bell, Langmuir 17 (2001) 4297–4303.
[67] B. Bachiller-Baeza, I. Rodriguez-Ramos, A. Guerrero-Ruiz, Langmuir 14 (1998) 3556–3564.
[68] Y. Tanaka, T. Iizuka, K. Tanabe, Journal of the Chemical Society, Faraday Transactions 178 (1982) 2215–2225.
[69] M.C. Muñoz, S. Gallego, J.I. Beltrán, J. Cerdá, Surface Science Reports 61 (2006) 303–344.
[70] A. Beretta, A. Donazzi, G. Groppi, P. Forzatti, V. Dal Santo, L. Sordelli, V. De Grandi, R. Psaro, Applied Catalysis B: Environmental 83 (2008) 96–109.